

An Analytical Contact Model for Design of Compliant Fingers

Chao-Chieh Lan¹

Department of Mechanical Engineering,
National Cheng Kung University,
No. 1 University Road,
Tainan 701, Taiwan
e-mail: cclan@mail.ncku.edu.tw

Kok-Meng Lee

Woodruff School of Mechanical Engineering,
Georgia Institute of Technology,
Atlanta, GA 30332-0405

A compliant gripper gains its dextral manipulation by the flexural motion of its fingers. It is a preferable device as compared to grippers with multijoint actuations because of reduced fabrication complexity and increased structural reliability. The prediction of contact forces and deflected shape are essential to the design of a compliant finger. A formulation based on nonlinear constrained minimization is presented to analyze contact problems of compliant fingers. The deflections by flexural and shear deformations are both considered. For a planar finger, this formulation further reduces the domain of discretization by one dimension. Hence, it offers a simpler formulation and is computationally more efficient than other methods such as finite element analysis. This method is rather generic and can facilitate design analysis and optimization of compliant fingers. We illustrate some of these attractive features with two types of compliant fingers, one for object handling and the other for snap-fit assembly applications.

[DOI: 10.1115/1.2803655]

Keywords: compliant finger, grippers, contact, constraint minimization

1 Introduction

Mechanical fingers have many applications in high-speed production automation. Unlike a typical multijoint finger actuated by one or more electrical or pneumatic motors, a compliant finger capable of large flexural deflection is manipulated primarily by means of its contact with the target being handled. The concept of compliant fingers has been widely used for snap-fit assembly. Bonenberger [1] has a comprehensive description on snap-fit assembly. Closed-form design equations based on the linear beam theory can be found in Refs. [2,3] and other design concepts in Refs. [4,5]. Compliant fingers are also applied to object handling to accommodate a limited range of shapes/sizes of live objects. Lee et al. [6] designed compliant rubber grippers (consist of multiple fingers) for singulating broilers for poultry meat production and later [7] exploited their application as graspers to automate transferring of live birds. As compliant rubber fingers are fatigue resistant, they have been widely used in automation applications that require repetitive motions, for example, poultry pickers and live bird harvesters. Recent research [8–11] explored compliant link contact to enhance motion transmission characteristics of *contact-aided compliant mechanisms*. As a compliant finger does not rely on multiple links that move relative to each other, it eliminates joint friction and yet requires no joint actuators. In addition, compliant fingers are easy to fabricate, assemble, and maintain. They have been shown to be more attractive than traditional multijoint fingers for high-speed automation involving natural objects.

Advance in microelectromechanical system (MEMS) has realized the need for mass production of microcomponents. Various micromachining methods have been developed, such as IC-based silicon processing, LIGA, surface machining, and microelectrodischarge machining (EDM). However, these techniques are only capable of two dimensional (2D) fabrication. In order to create broader applications based on MEMS devices, it is required to develop microgrippers for manipulating and assembling microcomponents for three dimensional (3D) applications. The interest to reduce the complexity of 3D assembly has motivated the de-

velopment of passive microgrippers. As compared to active microgrippers, which may be driven by means of electrothermal [12], electrostatic [13], electromagnetic [14], or piezoelectric [15] actuators, passive microgrippers mainly require contact between their compliant fingers and the microcomponent to generate motion required for assembly; examples include micromachined end effectors for MEMS assembly [16,17] and compliant microgrippers for microsnap-fit connector [18,19]. Since uncertain actuator displacement does not exist in passive microgrippers, they have significant potential for very high precision applications. However, design of a compliant gripper is more challenging due to the difficulty in predicting the contact-induced deflection of its fingers.

Compliant fingers undergo large deflection when they contact the target. In design, the deflected shape of the finger and the normal and tangential components of the contact forces (that must satisfy the boundary conditions at the interface) must be analyzed. Since most contact problems involving large deformation do not permit closed-form solutions, designers have resorted to numerical methods to approximate solutions. Among them, the *matrix inversion method* satisfies boundary conditions at specified matching points. It has been used by Paul and Hashemi [20] to calculate normal contact forces. Another method, the *variational inequality method*, determines the shape and size at contact by using well-developed optimization techniques. Fichera [21], and Duvant and Lions [22] have investigated on the existence and uniqueness of solution to contact problems. They show that the true contact area and surface displacement are those that minimize the total strain energy. From a numerical perspective, Kalker [23] formulates the minimization problem as a quadratic programming problem to solve frictionless non-Hertzian contact problems. The above two methods are based on the elastic half-space model [24] so that the linear elasticity theory holds. For contact problems involving large deformation, a more general approach, the *finite element method* (FEM), is widely used. However, its formulation is complicated and often requires intensive computation. Alternatives to the FEM are also found in the literature. Yin and Lee [25] proposed a numerical solver based on elliptical integrals to solve the problem of a large-deflected finger contacting an elliptic object. By assuming only one contact point exists, the results agree well with those obtained by using FEM with less computation time. However, the solver models the finger as a one dimensional segment without considering the thickness of the finger. Hence, it is not applicable

¹Corresponding author.

Contributed by the Mechanisms and Robotics Committee of ASME for publication in the JOURNAL OF MECHANICAL DESIGN. Manuscript received July 27, 2006; final manuscript received February 9, 2007; published online December 7, 2007. Review conducted by Qizheng Liao.

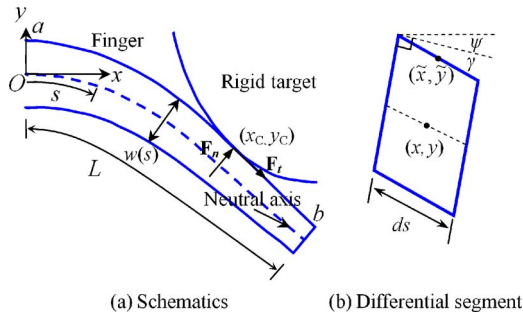


Fig. 1 Compliant gripping contacts

to thick fingers. Other research focuses on modeling the stiffness of soft finger at contact using a set of line springs (see Ref. [26], for example).

As the contact force and contact point are essential for compliant finger design, they are not easy to obtain. Simple closed-form equations [2,3] may be insufficient for sophisticated design. More refined analysis techniques such as FEM are also available but they often improve accuracy at the expense of significantly more computation effort and time. Motivated by the need to design compliant fingers efficiently without loss of accuracy, this paper presents a computational model using nonlinear constrained minimization (NCM) to facilitate the design of compliant fingers. This model is rather general and can be used to analyze contact between an arbitrarily shaped 2D target and a compliant finger with arbitrary geometry in its lateral direction. Two of the key components to this model are the expression of strain energy and formulation of geometric constraints. This remaining paper offers the following:

1. The model presented here extends the classical beam theory by relaxing the assumption of small deflection and accounts for both flexural and shear deformations.
2. The principle of minimum potential energy with contact constraints is applied to solve the contact problem. This (NCM) formulation reduces the 2D contact problem to 1D while taking the geometric shape of the finger into consideration.
3. A numerical method based on sequential quadratic programming is presented for solving the constraint minimization problem.
4. Two illustrative examples compare the computed results of the proposed model against those obtained using FEM; the results are in excellent agreement with simpler formulation and much less computation effort.

2 Contact Model With Compliant Fingers

The contact problem involving compliant fingers is formulated as a constrained minimization. The formulation begins with the strain energy of a compliant finger capable of large deflection with shear deformation. This is followed by formulating the contact constraints that prevent the finger from penetrating the target. The minimization of the strain energy subject to contact constraints forms a nonlinear constrained optimization problem, which is solved numerically for the deflected shape of the finger. Normal and tangential components of the contact forces can then be obtained by using Newton's third law.

2.1 Finger Model. Figure 1(a) shows a typical contact geometry involving a compliant finger, the manipulation of which relies on contact forces from the rigid target that deflects the finger and accommodates the target geometry. The finger model developed here relaxes the assumption of small deflection commonly made in thin beam theories (such as Euler–Bernoulli's or Timoshenko's

[27]). The finger is modeled in terms of the differential arc length ds along the neutral axis (represented by the dash line) instead of dx so that it is applicable to large flexural deflections.

The deformation of the finger (with varying thickness w) is described by the angle of rotation ψ and shear angle γ . As shown in Fig. 1(b), the deflection of a differential segment can be interpreted as a superposition of two effects:

- a bending moment induces an angle of rotation ψ without changing the shear angle and
- a shear force distorts the segment by a shear angle γ without causing it to rotate.

The resultant of these effects is that the cross section rotates by a total angle of $\psi + \gamma$. The position of a point (x, y) on the neutral axis can be obtained as

$$\begin{bmatrix} x(\hat{s}) \\ y(\hat{s}) \end{bmatrix} = \int_0^{\hat{s}} \begin{bmatrix} \cos(\psi + \gamma) \\ \sin(\psi + \gamma) \end{bmatrix} ds \quad (1)$$

where \hat{s} is the arc length from origin O to point (x, y) .

We consider here quasistatic analysis (see, for example, Ref. [28] for an experimental justification) and apply the principle of minimum total potential energy on the finger/target pair. Two assumptions are made throughout this paper:

1. The contact between the finger and target is regarded as adhesionless. Contact surface deformation of the finger is ignored (treated as rigid surface) since it is relatively small compared to bending and shear (see Ref. [28], for example). Hence, the virtual displacement and the corresponding virtual work done by traction forces on the contact surface are considered to be zero. The total potential energy only includes the strain energy from the deflected finger.
2. The finger and target surfaces obey Coulomb's friction law and are sliding on each other. The magnitude of normal force $|\mathbf{F}_n|$ and friction force $|\mathbf{F}_t|$ are then related to each other by $\mu|\mathbf{F}_n| = |\mathbf{F}_t|$, where μ is kinetic friction coefficient.

2.2 Minimization of Strain Energy With Contact Constraints. The strain energy V stored in the deflected finger can be stated as [29]

$$V = \frac{1}{2} \int_0^L \left\{ EI(s) \left(\frac{d\psi}{ds} \right)^2 + \kappa GA(s) [\gamma(s)]^2 + EA(s) \left(\frac{de}{ds} \right)^2 \right\} ds \quad (2)$$

where s is the arc length; e is the axial displacement; A , L , and I are the cross-section area, length, and moment of inertia of the finger, respectively; E and G are Young's and shear moduli of the finger, respectively; and κ is the shear coefficient.

The shear coefficient κ is introduced to correct the assumption that the shear angle remains constant in each cross section (no warp). In Eq. (2), the first and second terms in the integral account for the strain energy due to linear elastic bending and shear, respectively. The third term accounts for the axial deformation. However, it is usually very small for compliant-finger contact applications where manipulation relies mostly on flexural rather than axial deflection [29,30]. Hence, it is neglected hereafter.

The prescribed boundary constraint for a finger clamped at the origin is

$$\psi(0) = \Psi_0 \quad (3)$$

where Ψ_0 is the initial angle of rotation at $s=0$. In addition, there are contact constraints that describe the state at contact. Specifically, a point (\tilde{x}, \tilde{y}) on the contact surface ab shown in Fig. 1(a) and a point (\bar{x}, \bar{y}) on the target surface must satisfy either of the following inequalities in order not to penetrate each other:

$$g(\tilde{x}, \tilde{y}) \geq 0 \quad (4a)$$

$$g(\bar{x}, \bar{y}) \geq 0 \quad (4b)$$

The gap function g describes the target surface in Eq. (4a) and finger surface in Eq. (4b). The functions ψ and γ must follow the prescribed boundary constraint in Eq. (3) and contact constraints in Eq. (4) in order to be kinematically admissible.

The principle of minimum potential energy states that of all kinematically admissible deformations, those that satisfy the equilibrium condition at contact make the total potential energy minimum. With this, we find the minimum of V from Eq. (2) with kinematical constraints imposed by Eqs. (3) and (4). Note that when using the principle of minimum potential energy, we only need to account for the prescribed boundary condition (Eq. (3)). The natural boundary condition is automatically satisfied inside the energy integral (Eq. (2)). Thus, the resulting ψ and γ will yield the deflected shape of the finger at contact. The numerical solutions are presented next to obtain the deflected shape.

3 Numerical Solutions

The procedures to obtain the numerical solutions begin with finite difference approximations of Eqs. (2) and (4), then solve the minimization problem for the finger shape using the method of sequential quadratic programming, and finally obtain the contact forces.

3.1 Approximation of the Strain Energy. The neutral axis of the finger is discretized into N equally spaced intervals so that

$$s_i = i\Delta s \quad \Delta s = \frac{L}{N} \quad \psi_i \approx \psi(s_i) \quad \gamma_i \approx \gamma(s_i)$$

$$x_i \approx x(s_i) \quad y_i \approx y(s_i) \quad i = 0 \sim N$$

Hence, Eq. (2) can be approximated by, but not restricted to, the trapezoidal rule.

$$V \approx \frac{1}{2} \Delta s \left[\sum_{i=1}^N EI_{i-1/2} \left(\frac{\psi_i - \psi_{i-1}}{\Delta s} \right)^2 + \kappa GA_{i-1/2} \left(\frac{\gamma_i + \gamma_{i-1}}{2} \right)^2 \right] \quad (5)$$

The area A and moment of inertia I are approximated as

$$I_{i-1/2} = \frac{I(s_i) + I(s_{i-1})}{2} \quad \text{and} \quad A_{i-1/2} = \frac{A(s_i) + A(s_{i-1})}{2}$$

Since the finger is clamped at the base, the initial angle of rotation (ψ_0) is equal to Ψ_0 . As will be shown in an example in Sec. 4, the functions ψ and γ experience nonsmoothness at the contact point when the contact forces directly exert on the peripheral of the finger. Hence, polynomial approximations (where the functions are assumed to be continuously differentiable) are less appropriate in $s \in [0, L]$ since the contact point is not known in advance.

From Eq. (1), any point on the neutral axis can be approximated as

$$x_i = \frac{1}{2} \sum_{k=0}^{i-1} [\cos(\psi_k + \gamma_k) + \cos(\psi_{k+1} + \gamma_{k+1})] \Delta s$$

and

$$y_i = \frac{1}{2} \sum_{k=0}^{i-1} [\sin(\psi_k + \gamma_k) + \sin(\psi_{k+1} + \gamma_{k+1})] \Delta s$$

Any point (\bar{x}, \bar{y}) on the contact surface ab of the finger is related to its corresponding point on the neutral axis by

$$\begin{bmatrix} \bar{x} \\ \bar{y} \end{bmatrix} = \begin{bmatrix} x \\ y \end{bmatrix} + \frac{w(s)}{2} \begin{bmatrix} \cos(\psi + \gamma + \pi/2) \\ \sin(\psi + \gamma + \pi/2) \end{bmatrix} \quad (6)$$

where $w(s)$ in Eq. (6) accounts for nonuniform fingers. Point (\bar{x}, \bar{y}) is then used to formulate contact constraints in Sec. 3.2.

Special Case: Compliant Finger With a Rigid Jaw. Some fin-

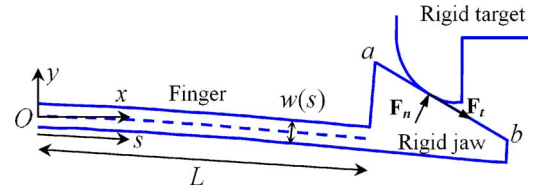


Fig. 2 Grip with a rigid jaw

gers (such as snap fits) have a rigid jaw attached to the end of the finger (as shown in Fig. 2), where the contact occurs between the jaw and target. Note that the length L here does not include the size of the jaw. Since the contact force does not act at the compliant part of the finger, the deflected finger shape can be approximated by continuously differentiable polynomials, i.e.,

$$\psi \approx \sum_{i=0}^k c_i s^i$$

and

$$\gamma \approx \sum_{i=0}^k d_i s^i \quad (7)$$

where c_i and d_i are coefficients.

The strain energy is obtained by plugging Eq. (7) into Eq. (2) as

$$V \approx \frac{1}{2} \int_0^L \left\{ EI(s) \left[\sum_{i=1}^k i c_i s^{i-1} \right]^2 + \kappa GA(s) \left[\sum_{i=0}^k d_i s^i \right]^2 \right\} ds \quad (8)$$

After integration, Eq. (8) becomes a quadratic function of c_i 's and d_i 's. Similarly, the points on the neutral axis can be obtained by inserting Eq. (7) into Eq. (1) as

$$x(\hat{s}) \approx \int_0^{\hat{s}} \cos \left(\sum_{i=0}^k c_i s^i + d_i s^i \right) ds$$

and

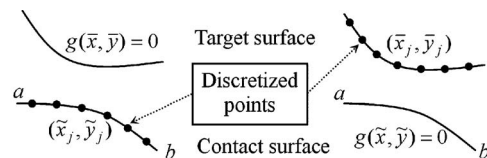
$$y(\hat{s}) \approx \int_0^{\hat{s}} \sin \left(\sum_{i=0}^k c_i s^i + d_i s^i \right) ds$$

The position (\bar{x}, \bar{y}) on the contact surface of the jaw, i.e., segment ab , can be described by the angle of rotation at $s=L$ and the point $[x(L), y(L)]$:

$$\begin{bmatrix} \bar{x} \\ \bar{y} \end{bmatrix} = \begin{bmatrix} x_L \\ y_L \end{bmatrix} + \begin{bmatrix} \cos(\psi_L + \gamma_L) & \sin(\psi_L + \gamma_L) \\ -\sin(\psi_L + \gamma_L) & \cos(\psi_L + \gamma_L) \end{bmatrix} \begin{bmatrix} \mathbf{P}_x \\ \mathbf{P}_y \end{bmatrix} \quad (9)$$

where the subscript L denotes the value obtained at $s=L$; $[\mathbf{P}_x, \mathbf{P}_y]^T$ is the position vector from (x_L, y_L) to (\bar{x}, \bar{y}) in the jaw frame (with origin at $[x_L, y_L]^T$ and axes parallel to x - y before contact).

3.2 Discretization of Contact Constraints. Two formulations are illustrated for discretizing the constraints in Eq. (4). As shown in Fig. 3(a), the first discretizes the known contact surface into M points, whose positions are obtained using Eq. (6) or (9). The constraint function g then describes the target surface. The



(a) Discretized contact surface (b) Discretized target surface

Fig. 3 Formulation of constraint functions

second shown in Fig. 3(b) discretizes the target surface into M points and the constraint function g then describes the contact surface. The following inequalities must hold for discretized contact and target surfaces, respectively:

$$g(\bar{x}_j, \bar{y}_j) \geq 0 \quad j = 1 \sim M \quad (10a)$$

$$g(\bar{x}_j, \bar{y}_j) \geq 0 \quad j = 1 \sim M \quad (10b)$$

The choice between the two formulations depends on which surface is smoother or which can be described by a continuous function g . The surface with a sharper corner is always the discretized surface.

3.3 Sequential Quadratic Programming. To solve for the deflected shape of the finger due to contact, the quadratic object functions, Eqs. (5) and (8), must be minimized subject to inequality constraints in Eq. (10). For this, the sequential quadratic programming (SQP) is presented here to solve for the minimum. Specifically, the problem is rewritten as follows:

$$\min f(\mathbf{x})$$

subject to

$$h(\mathbf{x}) = 0 \quad g_j(\mathbf{x}) \geq 0 \quad j = 1 \sim M \quad (11)$$

where f denotes the strain energy, \mathbf{x} is the vector of (c_i, d_i) for indirect contact or (ψ_j, γ_j) for direct contact, h is the prescribed boundary condition, and g_j is the j th inequality constraint. The SQP approximates the current state (say, \mathbf{x}_k) by a quadratic programming (QP) subproblem as

$$\min \frac{1}{2} \mathbf{p}^T \nabla^2 L(\mathbf{x}_k) \mathbf{p} + \nabla f(\mathbf{x}_k)^T \mathbf{p}$$

subject to

$$\nabla h(\mathbf{x}_k) \mathbf{p} + h(\mathbf{x}_k) = 0 \quad (12)$$

$$\nabla g_j(\mathbf{x}_k) \mathbf{p} + g_j(\mathbf{x}_k) \geq 0 \quad j = 1 \sim M$$

where

$$\mathbf{p} = \mathbf{x} - \mathbf{x}_k \quad \text{and} \quad L = f(\mathbf{x}) + \sum_{j=1}^M \lambda_j g_j(\mathbf{x}) + \lambda_{M+1} h(\mathbf{x})$$

The λ_j 's are Lagrange multipliers for the equality and inequality constraints in Eq. (11). Equation (12) contains a quadratic approximation of $f(\mathbf{x})$ and linear approximations of $h(\mathbf{x})$ and $g_j(\mathbf{x})$. The minimizer of Eq. (12) is then used to define a new state by setting $\mathbf{x}_{k+1} = \mathbf{x}_k + \mathbf{p}$. The minimizer of the QP should be the optimal solution of Eq. (11) when the iterative process converges. However, the computation of Hessian matrix $\nabla^2 L(\mathbf{x}_k)$ is time consuming for large problems and that it may not be positive definite. Various quasi-Newton algorithms can be used to approximate Hessian matrix. Here the popular by Bryoden–Fletcher–Goldfarb–Shanno (BFGS) algorithm is applied with formulas stated as follows [31]:

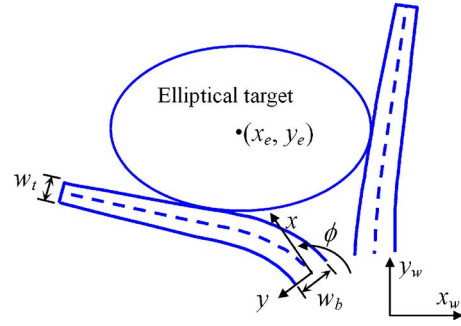


Fig. 4 Schematic of a rotating gripper contacting a target

$$\tilde{\mathbf{W}}_{k+1} = \tilde{\mathbf{W}}_k + \frac{\mathbf{q}_k \mathbf{q}_k^T}{\mathbf{q}_k^T \mathbf{p}_k} - \frac{\tilde{\mathbf{W}}_k \mathbf{p}_k \mathbf{p}_k^T \tilde{\mathbf{W}}_k}{\mathbf{p}_k^T \tilde{\mathbf{W}}_k \mathbf{p}_k} \quad (13)$$

where

$$\mathbf{p}_k = \mathbf{x}_{k+1} - \mathbf{x}_k \quad (13a)$$

and

$$\mathbf{q}_k = \nabla f(\mathbf{x}_{k+1}) - \nabla f(\mathbf{x}_k) + \nabla \sum_{j=1}^M \lambda_{k+1,j} [g_j(\mathbf{x}_{k+1}) - g_j(\mathbf{x}_k)] + \nabla \lambda_{k+1,M+1} [h(\mathbf{x}_{k+1}) - h(\mathbf{x}_k)] \quad (13b)$$

The matrix $\tilde{\mathbf{W}}_{k+1}$ is the approximation Hessian for the next step. The computational steps for the SQP are outlined as below.

1. Given initial \mathbf{x}_0 , $\tilde{\mathbf{W}}_0$, and tolerance ε :
2. For $k=0, 1, 2, \dots$
 - Solve Eq. (12) for \mathbf{p} and $\lambda_{k+1,j} (j=1 \sim M+1)$
 - Set $\beta=1$ and $\mathbf{x}_{k+1} = \mathbf{x}_k + \beta \mathbf{p}$
 - While $f(\mathbf{x}_{k+1}) > f(\mathbf{x}_k)$
 - $\beta = \beta/2$
 - $\mathbf{x}_{k+1} = \mathbf{x}_k + \beta \mathbf{p}$
 - End
 - Obtain BFGS update matrix $\tilde{\mathbf{W}}_{k+1}$ from Eq. (13).
 - If $|f(\mathbf{x}_{k+1}) - f(\mathbf{x}_k)| < \varepsilon$, exit
 - End

3.4 Determination of Normal and Tangential Contact Forces. Once the deflected shape is obtained, the contact forces are calculated for evaluating the performance of the finger. Applying Newton's third law, the contact forces $\mathbf{F} = [F_x, F_y]^T$ from the finger to the target (or $-\mathbf{F}$ from the target to the finger) must have a moment on the finger that equals the reaction moment at O :

Table 1 Simulation parameters and values

Parameters	Values	Parameters	Values
Young's modulus	$4.8 \times 10^6 \text{ N/m}^2$	Ellipse position y_e	0.12065 m
Shear modulus	$1.71 \times 10^6 \text{ N/m}^2$	(N, M)	(90,90)
Poisson's ratio	0.4	Contact elements and analysis type	CONTA171 and TARGET169; Surface-to-surface analysis
Base thickness w_b	0.030 m	Number of elements for finger	90×12
Tip thickness w_t	0.017 m	Solid element for ANSYS	PLANE2 for ellipse and PLANE42 for finger
Width	0.025 m		
Ellipse long axis	0.09906 m		
Ellipse short axis	0.06731 m		

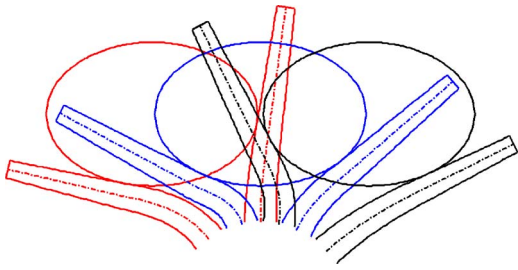


Fig. 5 Snapshots of finger-ellipse contact ($\phi=126$ deg, 102 deg, 78 deg from left to right)

$$EI(s) \frac{d\psi}{ds} \Big|_{s=0} = -\mathbf{P}_C \times \mathbf{F} \quad (14)$$

where $\mathbf{P}_C=[x_C y_C]^T$ is the contact point. The contact force \mathbf{F} includes normal and tangential components that are written in the following form:

$$\mathbf{F} = [F_x F_y]^T = \mathbf{F}_n + \mathbf{F}_t = [F_{nx} F_{ny}]^T + [F_{tx} F_{ty}]^T$$

The direction of normal contact force is parallel to the gradient of the target surface at contact point \mathbf{P}_C :

$$\frac{\partial g / \partial y}{\partial g / \partial x} \Big|_{(x_C, y_C)} = \frac{F_{ny}}{F_{nx}} \quad (15)$$

Since normal contact force and tangential (friction) contact force are orthogonal to each other, it must hold that

Table 2 Comparison of computation time

Method	Time (sec)
NCM (MATLAB)	17.60
FEM (ANSYS)	222.42

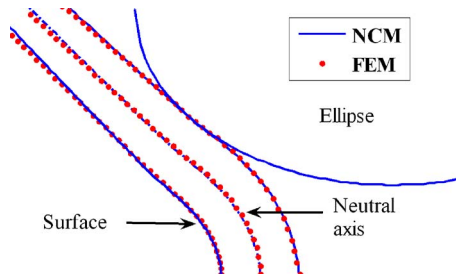


Fig. 6 Comparison of deflected shape at $\phi=90$ deg

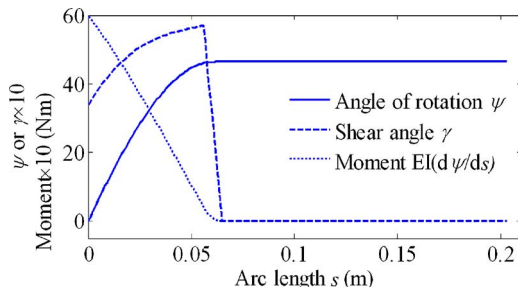


Fig. 7 Angle of rotation and shear angle at $\phi=90$ deg

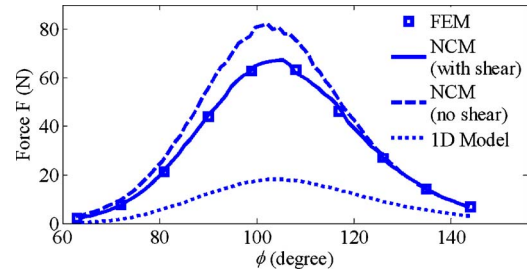


Fig. 8 Comparison of simulation results ($\mu=0$)

$$F_{nx} F_{tx} = -F_{ny} F_{ty} \quad (16)$$

Since the contact surface is slipping, the magnitude of normal force relates to the magnitude of friction force by

$$\mu \sqrt{F_{nx}^2 + F_{ny}^2} = \sqrt{F_{tx}^2 + F_{ty}^2} \quad (17)$$

where μ is the kinetic friction coefficient. The components F_{nx} , F_{ny} , F_{tx} , and F_{ty} can be solved simultaneously from Eqs. (14)–(17). Note that the signs of F_{tx} and F_{ty} have to be determined from the direction of interaction between the finger and target.

4 Verification of Frictionless and Frictional Contacts

Two examples are illustrated here, which also offer a means to verify the formulation introduced in Sec. 2, where FEM serves a basis for comparison. Both frictionless and frictional contacts will be considered. In Example I, a gripper manipulates an elliptical target by direct finger contacts. Such target handling applications can be seen in Refs. [6,32].

To show applications of designing snap fits for part assembly, Example II illustrates a finger that contacts the target through a rigid jaw. Two target geometries are illustrated in this example, namely, a smooth and a sharp-corner targets; the latter is not continuously differentiable. For clarity, the compliant portion of the finger is assumed to be thin and hence shear deformation is not considered.

Example I: Finger for Target Handling. As shown in Fig. 4, this example studies the effect of finger geometry and shear deformation of rotating fingers on manipulating an elliptical target by direct contact. Two symmetric sets of grippers are required on both sides of the ellipse with the long axis of the ellipse the line of symmetry. For clarity, only one set of such gripper is shown in Fig. 4. The two sets of grippers provide a net force in the x_w direction for transferring the target (the force in the y_w direction and moment in the z_w direction are canceled). Each gripper has two nonuniform (identical) fingers with 36 deg apart before deflection. We consider the left finger and perform a quasistatic analysis where the relationship between the target and rotating finger can be described by

$$\phi = -236.22x_e + 102 \text{ deg} \quad (18)$$

where x_e (in meters) is the center of the target and ϕ is the rotation of the finger. Both are measured in the world frame x_w, y_w . The

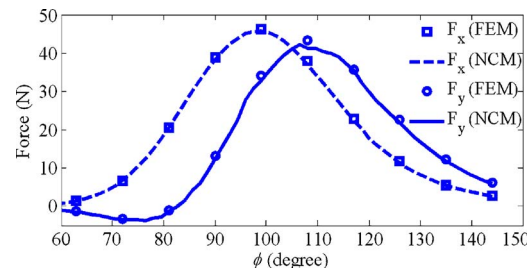


Fig. 9 Comparison of simulation results ($\mu=0.5$)

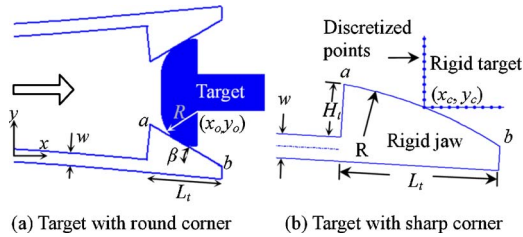


Fig. 10 Gripping for snap-fit assembly

contact surface includes one side of the finger that approaches the target. Since the contact location is an unknown, the whole finger surface is discretized and the gap function g is obtained by using the equation of an ellipse:

$$g_j = b_1 \bar{x}_j^2 + b_2 \bar{y}_j^2 + b_3 \bar{x}_j \bar{y}_j + b_4 \bar{x}_j + b_5 \bar{y}_j + b_6 \geq 0 \quad (19)$$

where b_i 's are the coefficients of the elliptical target.

Various shear coefficient formulae have been proposed for the shear coefficient κ in Eq. (2). We adopt the formula suggested by Kaneko [33] to correct the shear angle of the finger with a rectangular cross section, which is

$$\kappa = (5 + 5\nu)/(6 + 5\nu) \quad (20)$$

where ν is Poisson's ratio. The results of the NCM and FEM are compared with simulation parameters listed in Table 1. Figure 5 shows three continuous snapshots where the elliptical target moves from left to right while the gripper rotates clockwise. The computation time of $x_o=0.0508$ m is compared in Table 2 where both NCM and FEM are computed using a Pentium 4 PC (2.8 GHz with 512 MByte memory). The corresponding deflected shapes (at $\phi=90$ deg) of both methods are also compared in Fig. 6. For the NCM, the computed angle of rotation ψ and shear angle γ are plotted in Fig. 7. There is a jump for $EI(d\psi/ds)$ and γ around $s=0.05$ m where the contact point locates. There is no deformation after the contact point and hence, ψ remains constant and γ becomes zero. Figure 8 compares the results of frictionless contact by using the NCM, FEM, and one dimensional (1D) model (where the finger is treated as a line segment without considering its lateral thickness). In Fig. 9, the results of frictional contact are also compared with direction of friction force \mathbf{F}_f pointing to the negative x axis.

For living targets, the contact force profiles shown in Figs. 8 and 9 are very important since excessive forces will damage the target. Through NCM simulations, the contact force profile can be predicted, which will reduce the number of design configurations to be tested and offer an essential basis for optimizing the finger geometry.

Example II: Finger for Snap-Fit Assembly. An effective snap-fit assembly often requires designing the finger geometry such that it is easy to insert but very difficult to pull out. We study here the effect of finger geometry and coefficient of friction on the insertion forces. Two jaw geometries are illustrated here; (a) smooth target surface and (b) nonsmooth target surface shown in Figs. 10(a) and 10(b), respectively. Due to symmetry, only the bottom

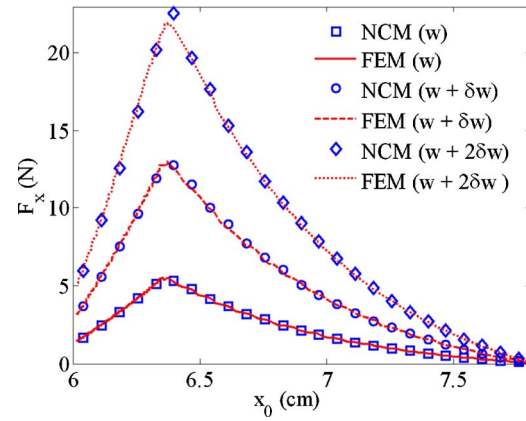


Fig. 11 Effect of thickness on insertion force (Example II(a); $\mu=0$, $w=0.0032$ m and $\delta w=0.001$ m)

finger is considered.

(a) *Finger With a Smooth Target Surface.* Consider the finger/target geometry shown in Fig. 10(a). Since the target surface is smooth, Eq. (10a) is applied by discretizing contact surface ab into M equally spaced points. The constraint function describing the target surface at contact is characterized by the equation of a circle such that

$$g_j(\bar{x}_j, \bar{y}_j) = (\bar{x}_j - x_o)^2 + (\bar{y}_j - y_o)^2 - R^2 \geq 0 \quad (21)$$

where R is the radius of the extrusion part of the target and (x_o, y_o) is center of the circle, as shown in Fig. 10(a). The simulation parameters are listed in Table 3. The results comparing NCM and FEM are shown in Figs. 11 and 12, which also illustrate the effects of different thicknesses and coefficient of friction on the insertion force (F_x), respectively. Both figures show excellent agreement between the NCM and FEM results. Figure 13 also shows the deflection shape obtained by ANSYS[®] where x_o

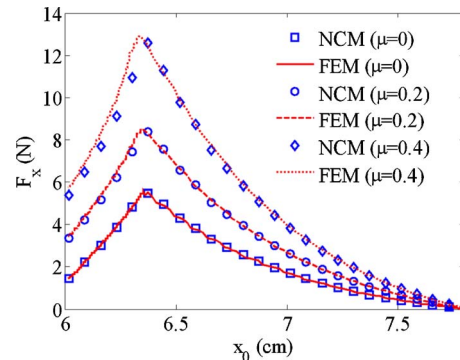


Fig. 12 Effect of friction on insertion force (Example II(a); $\mu=0, 0.2, 0.4$; $w=0.0032$ m)

Table 3 Simulation parameters and values of Example II(a)

Parameters	Values	Parameters	Values
Young's modulus	2.62×10^9 N/m ²	Element type for ANSYS	PLANE2 for finger and target
Lead angle β	25 deg	Contact elements and analysis type	CONTA175 and TARGET169; Node-to-surface analysis
Width	0.0095 m	M	50
Finger length L	0.057 m	a	(0.057 m, 0.0105 m)
Jaw length L_f	0.019 m	b	(0.0762 m, 0.0016 m)
Fixture radius R	0.0089 m		
Fixture position y_o	0.0105 m		

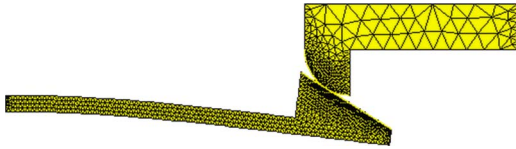


Fig. 13 Simulation results from FEM (Example II(a))

=0.06781 m. As Fig. 11 indicates, the maximum insertion force occurs at $x_o=0.064$ m and increases as thickness increases. Such property is very useful for designing snap fits whose performance are dominated by F_x .

(b) *Finger With a Nonsmooth Target Surface.* Figure 10(b) shows a target that has a sharp corner at (x_c, y_c) , which is not continuously differentiable. Applying Eq. (10b), the target surface is discretized and a circle function is used to describe arc ab . The simulation parameters are listed in Table 4 and the results are in Fig. 14. As shown in Fig. 15, the insertion forces computed for three friction coefficients ($\mu=0, 0.2, 0.4$) agree with the FEM results before the maximum insertion force occurs (around $x_c=0.058$ m). When the target (x_c, y_c) reaches point a , FEM has excess element distortion around the corner and leads to divergence. The NCM, on the other hand, does not suffer from this problem and can predict the constant insertion force at the end of insertion.

Table 4 Simulation parameters and values of Example II(b)

Parameters	Values	Parameters	Values
Young's modulus	2.62×10^9 N/m ²	Jaw radius R	0.05 m
Thickness w	0.0032 m	Target position y_c	0.0026 m
Width	0.0095 m	M	20
Finger length L	0.057 m	a	(0.057 m, 0.0085 m)
Jaw length L_j	0.019 m	b	(0.076 m, 0.0016 m)
Jaw height H_j	0.0069 m		

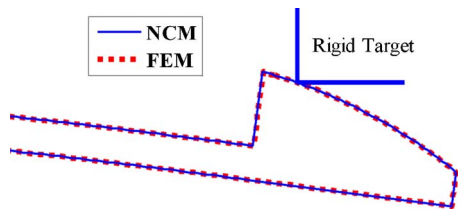


Fig. 14 Comparison of deflected shape at $x_c=0.0612$ m (Example II(b))

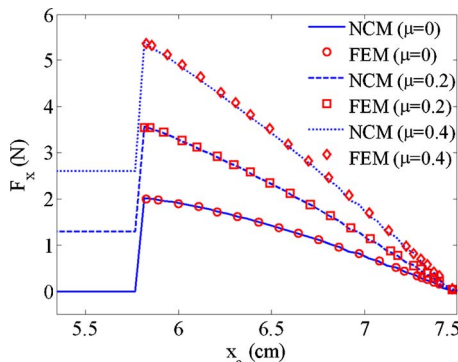


Fig. 15 Insertion force of Example II(b)

Table 5 Comparison of computation time

Method	Example II(a)	Example II(b)
NCM (MATLAB)	2.31 s (fourth order poly.)	1.64 s (fourth order poly.)
FEM (ANSYS)	516.46 s (1266 elements)	547.76 s (1377 elements)

Table 5 lists the average computation time for calculating the insertion force at $x_o=0.0678$ m and $x_c=0.0582$ m for Examples II(a) and II(b), respectively. For both cases, the FE mesh sizes of the finger surface are 100 and 50 for contact surface ab . The mesh sizes are chosen for accuracy and convergence considerations. It shows that the formulation presented here is computationally more efficient and stable without losing accuracy. The NCM for both cases converges when using polynomials (Eq. (7)) higher than fourth order. As a guideline, the minimum order polynomial is four for small to median deflection. For fingers with larger deflection, higher order polynomials are expected.

To obtain a better snap-fit design, the maximum insertion and retention forces must be chosen properly so that it is easy to assemble and detach without losing integrity of the assembly. Figures 11, 12, and 15 in Example II indicate the values of maximum insertion forces (F_{max}) and location where it occurs. The force F_{max} depends on the mating geometry and coefficient of friction of the finger-target pair. Equations that based on classical beam theory have been provided [2,3] to quickly obtain these forces for fingers with simple geometry and undergoing small deflection. As these equations provide only first-order accuracy, the NCM has been demonstrated (in the previous two examples) to accurately predict F_{max} for large-deflected fingers with complicated geometry. Consider the finger shown in Fig. 10(b) as an illustration. The relationship between F_{max} and finger geometry is obtained by using NCM when $\mu=0$. The result shown in Fig. 16 indicates that F_{max} can be increased by increasing the thickness w of the finger or dimension H_j of the jaw. Thus the proposed NCM can immediately help practical designer choose appropriate finger dimensions without costly prototyping iterations.

Concluding Examples I and II, the following observations can be made from the comparison among NCM and other existing methods:

1. As shown in Fig. 8, the 1D model ignores the geometry and is only applicable for fingers with relatively small thickness. The error of contact forces increases as the thickness increases. In addition, when applying the NCM without considering shear deformation, the contact force profile tends to be higher than those that consider shear deformation. When considering shear deformation, the predicted contact forces match well with FEM. Typical differences are within 3%. Without losing accuracy, the NCM, which discretizes the

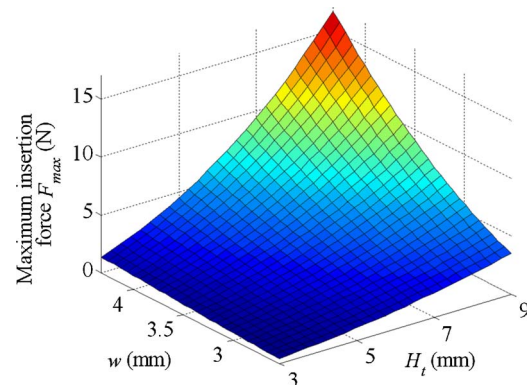


Fig. 16 Relations between the maximum insertion force and finger geometry (Example II(b); $\mu=0$)

finger in one dimension (along the neutral axis), can accurately account for both flexural and shear deformations that become significant for thick fingers. It is also far faster than methods that discretize the finger in two dimensions (along the neutral axis and transverse direction).

- The excellent agreement of the NCM and FEM also verifies that the assumption of negligible surface deformation for frictionless contact and frictional contact with moderate friction coefficient.
- In order to satisfy the boundary conditions of the finger/target surface, FEM requires discretization of both finger and target surfaces whereas the NCM needs only to discretize one of the surfaces and treat the other one as a continuous function. Hence, the formulation of NCM can be simpler. When modeling surfaces with sharp corners, NCM is also more stable while FEM may have excess element distortion.

5 Conclusions

A computational model based on NCM has been presented for analyzing compliant fingers whose manipulation primarily relies on direct or indirect contact with targets. The model takes into account large flexural deflection and shear deformation whose effect cannot be neglected for thick fingers. By formulating contact constraints this model can be applied to nonuniform fingers and with arbitrary target geometry.

Two examples have been presented to illustrate the formulation. Both frictionless and frictional contacts have been considered. The simulation results of the NCM agree well with those obtained by using FEM within 3% difference. The advantages of the NCM are the following: (a) The dimension of discretization can be reduced by one. Hence, it is computationally much more efficient. (b) Only one surface, either the target or contact surface, needs to be discretized. Hence, its formulation is simpler.

The excellent agreement shows that the formulation offered by the NCM can effectively facilitate the process of design and analysis of compliant fingers that have a broad spectrum of applications ranging from MEMS device fabrication [16–19] to automated handling of live objects in food processing industry [7]. In addition, the NCM has been illustrated in the context of 2D deflections to demonstrate the effect of bending and shear. However, the extension of this formulation to 3D deflections, though tedious, is relatively straight forward [34].

Acknowledgment

This project is jointly funded by Georgia Agriculture Technology Research Program and US Poultry and Eggs Association.

References

- Bonenberger, P. R., 2000, *The First Snap-Fit Handbook: Creating Attachments for Plastics Parts*, Hanser Gardner Publications, Cincinnati, OH.
- AlliedSignal Corporation, 1997, "Modulus Snap-Fit Design Manual," Allied-Signal Plastics, Morristown, NJ.
- Bayer Corporation, 1996, "Snap-Fit Joints for Plastics, A Design Guide," Polymer Division, Pittsburgh, PA.
- Suri, G., and Luscher, A. F., 2000, "Structural Abstraction in Snap-Fit Analysis," *ASME J. Mech. Des.*, **122**(4), pp. 395–402.
- Genc, S., Messler, R. W., and Gabriele, G. A., 2000, "A Method for Attachment Design Concept Development in Integral Snap-Fit Assemblies," *ASME J. Mech. Des.*, **122**(3), pp. 257–264.
- Lee, K.-M., Gogate, R., and Carey, R., 1998, "Automated Singulating System for Transfer of Live Birds," *IEEE International Conference on Robotics and Automation*, Leuven, Belgium, Vol. 4, pp. 3356–3361.
- Lee, K.-M., 2001, "Design Criteria for Developing an Automated Live-Bird Transfer System," *IEEE Trans. Rob. Autom.*, **17**(4), pp. 483–490.
- Mankame, N. D., and Ananthasuresh, G. K., 2004, "A Novel Compliant Mechanism for Converting Reciprocating Translation Into Enclosing Curved Paths," *ASME J. Mech. Des.*, **126**(4), pp. 667–672.
- Crane, N. B., Howell, L. L., Weight, B. L., and Magleby, S. P., 2004, "Compliant Floating-Opposing-Arm (FOA) Centrifugal Clutch," *ASME J. Mech. Des.*, **126**(1), pp. 169–177.
- Cannon, J. R., and Howell, L. L., 2005, "A Compliant Contact-Aided Revolute Joint," *Mech. Mach. Theory*, **40**, pp. 1273–1293.
- Mankame, N. D., Ananthasuresh, G. K., 2007, "Compliant Transmission Mechanism with Intermittent Contacts for Cycle-Doubling," *ASME J. Mech. Des.*, **129**(1), pp. 114–121.
- Salim, R., Wurmus, H., Harnisch, A., and Hulsberg, D., 1997, "Microgrippers created in microstructurable glass," *Microsyst. Technol.*, **4**, pp. 32–34.
- Kim, C. J., Pisano, A., and Muller, R., 1992, "Silicon-Processed Overhanging Microgripper," *J. Microelectromech. Syst.*, **1**, pp. 31–36.
- Suzuki, Y., 1996, "Flexible Microgripper and its Application to Micro-Measurement of Mechanical and Thermal Properties," *IEEE MEMS Proceedings Ninth Annual International Workshop*, pp. 406–411.
- Ansel, Y., Schmitz, F., Kunz, S., Gruber, H. P., and Popovic, G., 2002, "Development of Tools for Handling and Assembling Microcomponents," *J. Microelectromech. Microeng.*, **12**, pp. 430–437.
- Tsui, K., Geisberger, A. A., Ellis, M., and Skidmore, G. D., 2004, "Micromachined End-Effector and Techniques for Directed MEMS Assembly," *J. Microelectromech. Microeng.*, **14**, pp. 542–549.
- Chang, R. J., Wang, H. S., and Wang, Y. L., 2003, "Development of Mesoscopic Polymer Gripper System Guided by Precision Design Axioms," *Precis. Eng.*, **27**, pp. 362–369.
- Oh, Y. S., Lee, W. H., Skidmore, G. D., 2003, "Design, Optimization, and Experiments of Compliant Microgripper," *ASME IMECE*, Washington, DC.
- Dechev, N., Cleghorn, W. L., and Mills, J. K., 2004, "Microassembly of 3D Microstructures Using a Compliant, Passive Microgripper," *J. Microelectromech. Syst.*, **13**(2), pp. 176–189.
- Paul, B., and Hashemi, J., 1981, "Contact Pressure on Closely Conforming Elastic Bodies," *ASME J. Appl. Mech.*, **48**(3), pp. 543–548.
- Fichera, G., 1964, "Problemi elastostatici con vincoli unilaterale: il problema di Signorini con ambigue condizioni al contorno," *Atti Accad. Naz. Lincei, Mem., Cl. Sci. Fis., Mat. Nat., Sez. 1a*, **7**, pp. 91–140.
- Duvant, G., and Lions, J. L., 1972, *Les Inequations en Mecanique et en Physique*, Dunod, Paris.
- Kalker, J. J., and van Randen, Y., 1972, "A Minimum Principle for Frictionless Elastic Contact With Application to Non-Hertzian Half-Space Contact Problems," *J. Eng. Math.*, **6**, pp. 193–206.
- Johnson, K. L., 1987, *Contact Mechanics*, Cambridge University Press.
- Yin, X., and Lee, K.-M., 2002, "Modeling and Analysis of Grasping Dynamics of High Speed Transfer of Live Birds," *Second IFAC Conference on Mechatronic Systems*, Berkeley, CA.
- Ghafoor, A., Dai, J. S., and Duffy, J., 2004, "Stiffness Modeling of the Soft-Finger Contact in Robotic Grasping," *ASME J. Mech. Des.*, **126**(4), pp. 646–656.
- Timoshenko, S. P., 1922, "On the Transverse Vibrations of Bars of Uniform Cross-Section," *Philos. Mag.*, **43**, pp. 125–131.
- Lee, K.-M., Joni, J., and Yin, X., 2001, "Compliant Grasping Force Modeling for Handling of Live Objects," *IEEE International Conference on Robotics and Automation*, Seoul, Korea, Vol. 2, pp. 1059–1064.
- Lan, C.-C., Lee, K.-M., 2006, "Generalized Shooting Method for Analyzing Compliant Mechanisms With Curved Members," *ASME J. Mech. Des.*, **128**(4), pp. 765–775.
- Fertis, D. G., 1998, *Nonlinear Mechanics*, CRC, Boca Raton, FL.
- Bazaraa, M. S., Sherali, H. D., and Shetty, C. M., 1993, *Nonlinear Programming: Theory and Algorithms*, Wiley, New York.
- Shahinpoor, M., Bar-Cohen, Y., Simpson, J. O., and Smith, J., 1998, "Ionic Polymer-Metal Composites (IPMCs) as Biomimetic Sensors, Actuators and Artificial Muscles—A Review," *Smart Mater. Struct.*, **7**, pp. R15–R30.
- Kaneko, T., 1975, "On Timoshenko's Correction for Shear in Vibrating Beams," *J. Phys. D.*, **8**, pp. 1927–1936.
- Lan, C.-C., 2005, "Computational Models for Design and Analysis of Compliant Mechanisms," Ph.D., thesis, Georgia Institute of Technology.